Surface passivation of GaN and GaN/AlGaN heterostructures by dielectric films and its application to insulated-gate heterostructure transistors

Tamotsu Hashizume,[a] Shinya Ootomo, Takanori Inagaki, and Hideki Hasegawa
Research Center for Integrated Quantum Electronics (RCIQE), Hokkaido University, Sapporo 060-8628, Japan

(Received 19 January 2003; accepted 22 March 2003; published 5 August 2003)

We have systematically investigated effects of plasma processing, formation of Si-based dielectrics, and formation of a thin Al_2O_3 film on the chemical and electronic properties of GaN and GaN/AlGaN heterostructure surfaces. The surface treatment in H_2-plasma excited by electron-cyclotron-resonance (ECR) source, produced nitrogen-vacancy-related defect levels at GaN and AlGaN surfaces, while the ECR-N_2-plasma treatment improved electronic properties of the surfaces. The deposition of a SiO_2 film on GaN and AlGaN surfaces was found to induce high-density interface states, due to unexpected and uncontrollable oxidation reactions on the surfaces during the deposition process. In comparison, the SiN_x/GaN passivation structure prepared by ECR-plasma assisted chemical vapor deposition showed good interface properties with the minimum D_{it} value of $1\times10^{11}\,cm^{-2}\,eV^{-1}$. However, excess leakage currents governed by Fowler–Nordheim tunneling were observed in the $SiN_x/Al_{0.3}Ga_{0.7}N$ structure, due to a relatively small conduction band offset of 0.7 eV between SiN_x and $Al_{0.3}Ga_{0.7}N$. A novel Al_2O_3-based passivation structure was proposed and fabricated by molecular beam deposition of Al and subsequent ECR O_2-plasma oxidation. *In situ* x-ray photoelectron spectroscopy showed successful formation of the Al_2O_3 layer with a thickness of 3.5 nm and a large conduction band offset of 2.1 eV between Al_2O_3 and $A_{0.3}Ga_{0.7}N$. The GaN/AlGaN insulated-gate heterostructure field-effect transistors (IG HFETs) having the Al_2O_3-based passivation structure showed a good gate control of drain currents up to $V_{GS}=+3$ V and achieved drain saturation current of 0.8 A/mm. The observed maximum g_m value is 120 mS/mm. No current collapse was observed in the Al_2O_3 IG HFETs, indicating a remarkable advantage of the present Al_2O_3-based passivation structure. [DOI: 10.1116/1.1585077]

I. INTRODUCTION

Recent progress in high-power/high-frequency field-effect transistors (FETs) based on GaN and its related heterostructures has demonstrated that they are key devices for next-generation high-density communication systems. However, these devices still have surface/interface-related problems, including collapse in drain current,[1] excess gate leakage,[2,3] and aging of Schottky contacts.[4] Furthermore, the device processing involves various kinds of surface treatments and junction formation steps, which may introduce defects on the processed GaN and AlGaN surfaces. A surface passivation process consisting of a suitable surface treatment and the formation of the insulated gate (IG) and passivation structure can solve these problems. In this regard, understanding and controlling surface properties of GaN and GaN-based heterostructures are of utmost importance.

For a prepassivation process, it is important to investigate cleaning processes for GaN and AlGaN surfaces. However, there are a few reports on the processed surfaces such as chemically treated surfaces, plasma-treated surfaces, etc. King *et al.*[5] and Hartlieb *et al.*[6] have investigated wet and dry cleaning processes for GaN and AlN surfaces, and proposed the ammonia-based high-temperature chemical vapor process. Our group has investigated correlation between chemical and electronic properties of GaN and AlGaN surfaces after various types of surface treatments,[7–9] and reported that the surface treatment using N_2 plasma excited by electron-cyclotron-resonance (ECR) source was very effective in improving the electronic properties of GaN and AlGaN surfaces.[9]

For the final stage of surface passivation and insulated gate structures, the use of dielectric films is indispensable. In this regard, there have been several studies on the properties of metal–insulator–semiconductor (MIS) structures using GaN and the surface passivation of GaN/AlGaN heterostructure field effect transistors (HFETs). A pioneering work on the GaN MISFET using a SiN_x gate was reported by Binari *et al.*[10] They deposited a SiN_x film on GaN by radio-frequency (rf) plasma enhanced chemical vapor deposition. However, the devices displayed low transconductance (g_m) due to high-density interface states. Kawai and co-workers[11] have demonstrated good dc performance of the GaN IG FET using an epitaxial AlN layer as a gate dielectric. However, it is very difficult to suppress the leakage current through AlN because of the difficulty of growing high-quality AlN films.[12] Hashizume, Nakasaki and Hasegawa[13,14] demonstrated for the first time that good interface properties can be realized in SiN_x/GaN passivation structures prepared by the ECR-N_2 plasma treatment and ECR-assisted chemical vapor deposition (ECR CVD). Thereafter, SiN_x-based surface passivation

[a]Electronic mail: hashi@rciqe.hokudai.ac.jp

TABLE I. Values of band gap, dielectric constant, and breakdown field for $Al_{0.3}Ga_{0.7}N$ and some dielectrics.

	E_G (eV)	ε_S	Breakdown field (MV/cm)
$Al_{0.3}Ga_{0.7}N$	4.1	9.0–9.5	>5
SiO_2	9	3.9	10
Si_3N_4	5.0	7	10
Ga_2O_3	4.5	10	1–3
Ta_2O_5	5	10–20	>10
MgO	8	8–9	5
AlN	6.2	8.5	10–15
Al_2O_3	7–9	9–10	>10

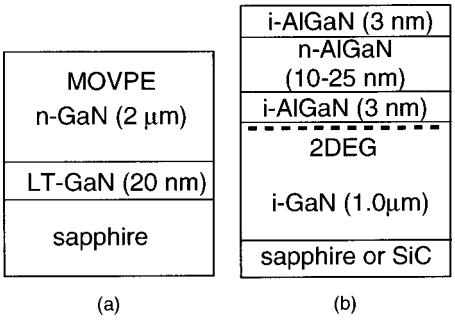

FIG. 1. Schematic illustrations of GaN and GaN/AlGaN heterostructure sample structures.

structures have been applied to the GaN/AlGaN HFETs.[1,15–19] Green *et al.*[15] and Lee *et al.*[16] reported the improvement of rf-power performance in the GaN/AlGaN HFETs. The reduction of current collapse was reported in the SiN_x IG GaN/AlGaN HFET,[17] or the SiN_x-passivated GaN/AlGaN HFETs.[1,18,19]

Other dielectrics such as SiO_2, Ga_2O_3, MgO and the native oxide of AlGaN have also been applied to the surface passivation of GaN and AlGaN surfaces. Therrien *et al.*[20] reported the passivation process including separate plasma oxidation of GaN and the deposition of thick SiO_2 film using remote plasma. Hong *et al.*[21] demonstrated that the $Ga_2O_3(Gd_2O_3)$/GaN system fabricated by molecular beam epitaxy (MBE) and electron beam evaporation showed low interface state densities. Gaffey *et al.*[22] reported good interface properties of the SiO_2/GaN structures prepared by jet vapor deposition. Inoue and co-workers[23] fabricated the IG AlGaN/GaN HFET using native oxide of AlGaN itself formed by thermal oxidation at 900 °C. Luo *et al.*[24] reported the passivation effects of the MBE-grown MgO films on the AlGaN/GaN HFETs.

In spite of these efforts, properties of insulator-semiconductor interfaces of GaN and AlGaN are not fully understood and successful surface passivation of GaN/AlGaN HFETs is not achieved.

In this article, we present a systematic investigation on effects of ECR-plasma processing and SiO_2- and SiN_x-based passivation on chemical and electrical properties of GaN and AlGaN surfaces. We used the ECR-plasma process for the surface treatments and the deposition of dielectrics, because it is a remote plasma process and it utilizes ions with low energies of 10 to several tens of eV. It is also shown that an Al_2O_3-based surface passivation structure drastically improves the electrical properties of GaN/AlGaN HFETs. Table I summarizes values of band gap, dielectric constant, and breakdown field for dielectrics previously applied or to be applicable to surface passivation of AlGaN. Those for $Al_{0.3}Ga_{0.7}N$ are also listed. Among them, Al_2O_3 is very attractive as an insulated gate for GaN/AlGaN HFETs because it has larger bandgap than that of $Al_{0.3}Ga_{0.7}N$, a high dielectric constant and a high breakdown electric field. Furthermore, Al_2O_3 is one of the native oxides of AlGaN. Thus, we developed the formation process of a thin Al_2O_3 layer on AlGaN by a combination of molecular beam deposition of Al and the subsequent ECR-O_2 plasma oxidation.

II. EXPERIMENT

A. GaN and GaN/AlGaN sample structures

Figure 1 shows schematic illustrations of GaN and GaN/AlGaN sample structures. High-quality epitaxial GaN wafers grown on sapphire substrates by metal organic vapor phase epitaxy (MOVPE) were used in this study. A buffer GaN layer (LT-GaN) was grown at low temperatures (500–550 °C) followed by the growth of a Si-doped GaN layer using SiH_4 as a dopant source at 1000 °C. Typical values of electron concentration and mobility of the Si-doped layer at room temperature (RT) is $2\times10^{17}\,cm^{-3}$ and 500 $cm^2/V\,s$, respectively.

The heterostructure samples grown by MOVPE consist of undoped GaN, undoped $Al_xGa_{1-x}N$, Si-doped $Al_xGa_{1-x}N$, and undoped $Al_xGa_{1-x}N$, as shown in Fig. 1(b). The Al content, *x*, ranged from 0.25 to 0.30. The samples showed clear Shuvnikov–de Haas oscillation in magnetoresistance characteristics at 2 K, and the electron concentrations determined from the Landau plots of the oscillation were in good agreement with the values obtained by the Hall measurement at the same temperature. These results clearly indicated the existence of two-dimensional electron gas (2DEG) at the GaN/AlGaN heterointerfaces. Typical values of the electron concentration and mobility of 2DEG at RT were $1.1\times10^{13}\,cm^{-2}$ and 900 $cm^2/V\,s$, respectively.

B. Surface passivation and device fabrication processes

The surface passivation process started from a simple wet treatment in organic solvents at RT and in an NH_4OH solution at 50 °C for 5–10 min. The NH_4OH treatment is effective in reducing natural oxides on GaN and AlGaN surfaces.[7,8]

For successful surface passivation of GaN and AlGaN surfaces, *in situ* processing and characterization were performed in the ultra-high-vacuum (UHV) multichamber system. All the chambers are connected to each other through a UHV tunnel chamber whose base pressure is 2×10^{-10} Torr.

For a pretreatment of the deposition of dielectric films, GaN and GaN/AlGaN surfaces were exposed to N_2 plasma or H_2 plasma excited by an ECR source with microwave (2.75 GHz) power of 50 W. The processing temperature and time were 280 °C and 1–5 min, respectively. The deposition of SiO_2 and SiN_x was performed at 280 °C by ECR CVD, using SiH_4 and N_2O as precursors for SiO_2 and SiH_4 and N_2 for SiN_x, respectively. The thickness of the deposited films ranged from 20 to 70 nm. We obtained refractive index values of 1.47 and 1.98 for the deposited SiO_2 and SiN_x films, respectively.

The device isolation was performed by an ECR-assisted reactive ion beam etching using a gas system consisting of CH_4, H_2, Ar, and N_2. The addition of N_2 to the gas system is very effective in achieving smooth and stoichiometric GaN and AlGaN surfaces even after the etching.[25] As an Ohmic contact, a Ti/Al/Ti/Au layered structure was deposited on the surfaces of GaN and GaN/AlGaN followed by the annealing at 600 °C for GaN and 800 °C for GaN/AlGaN for 2 min in N_2 ambient. A Ni/Au contact was used as a Schottky gate on GaN and AlGaN.

C. Characterization methods

The surface chemical properties of GaN and GaN/AlGaN samples were characterized by x-ray photoelectron spectroscopy (XPS). The XPS system is connected to the UHV multichamber system, thereby *in situ* XPS characterization of the processed GaN and GaN/AlGaN surfaces is available. The XPS measurement system (Perkin Elmer PHI 1600C) consists of a spherical capacitor analyzer and a monochromated Al $K\alpha$ x-ray source ($h\nu = 1486.6$ eV). The binding energies of the spectra were carefully calibrated through separate measurements of Cu $2p_{3/2}$, Ag $3d_{5/2}$, and Au $4f_{7/2}$ peak positions. Atomic force microscope (AFM) observation of GaN surfaces after various types of surface treatments was carried out using a Nanoscope II (Digital Instruments). Current–voltage ($I-V$) and capacitance–voltage ($C-V$) measurements were performed using HP 4156A semiconductor parameter analyzer and HP 4192A LF impedance analyzer, respectively.

III. RESULTS AND DISCUSSION

A. Effects of plasma processing on chemical and electronic properties of GaN and AlGaN surfaces

Figure 2 shows XPS Ga $3d$ and Al $2p$ spectra obtained from the air-exposed $Al_{0.25}Ga_{0.75}N$ surface. Both the Ga $3d$ and Al $2p$ peaks showed asymmetric features with shoulders at higher binding energies. We assigned these higher peaks to Ga_2O_3 and Al_2O_3, respectively. For deconvolution of the observed spectra, we have separately determined the peak energies and linewidths of the spectra in the Al_2O_3 and Ga_2O_3 phases, using a crystalline sapphire substrate and a sample prepared by oxidizing the metallic Ga layer, respectively. Both spectra include large amounts of oxides. This feature was responsible for the disorder in chemical composition, leading to the deterioration of surface electronic properties of GaN and AlGaN.[9]

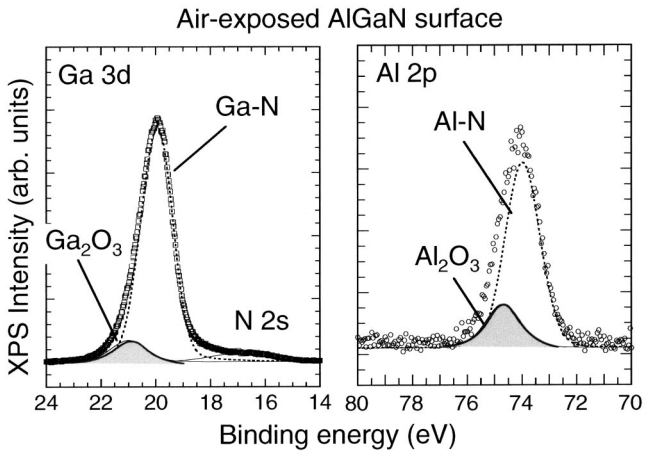

FIG. 2. XPS Ga $3d$ and Al $2p$ spectra obtained from the air-exposed $Al_{0.25}Ga_{0.75}N$ surface.

In order to remove the disordered layer including natural oxides, the ECR-assisted plasma treatments were employed on AlGaN surfaces. Figure 3 shows the integrated XPS intensities of O $1s$ and C $1s$ normalized by the N $1s$ intensity. After a wet treatment in NH_4OH solution, the O $1s$ intensity was reduced remarkably, because the Ga_2O_3 component can easily be dissolved in alkali solutions. However, the C $1s$ intensity remained almost unchanged. Both H_2- and N_2-plasma treatments at 280 °C for 1–5 min are effective in removing oxides and contamination from the AlGaN surface, as shown in Fig. 3.

However, the effects of the surface processing on electronic properties of GaN and AlGaN surfaces are very different between H_2-plasma and N_2-plasma treatments. The AFM images of the plasma-treated GaN surfaces are shown in Fig. 4. The ECR-N_2 plasma treated GaN exhibited a smooth surface with a root-mean-square (rms) roughness of 0.29 nm. The surface morphology showed the characteristic feature dominated by monolayer steps, and many of the steps were terminated by the large dark pits at the edges which could be

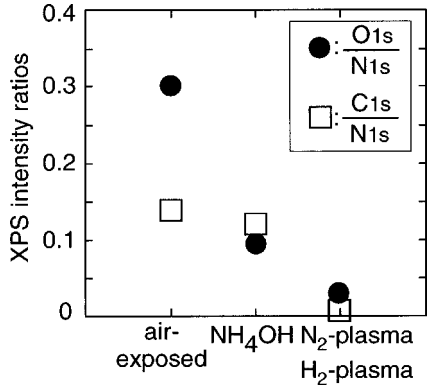

FIG. 3. Integrated XPS intensities of O $1s$ and C $1s$ normalized by the N $1s$ intensity at the AlGaN surface for the different surface treatments.

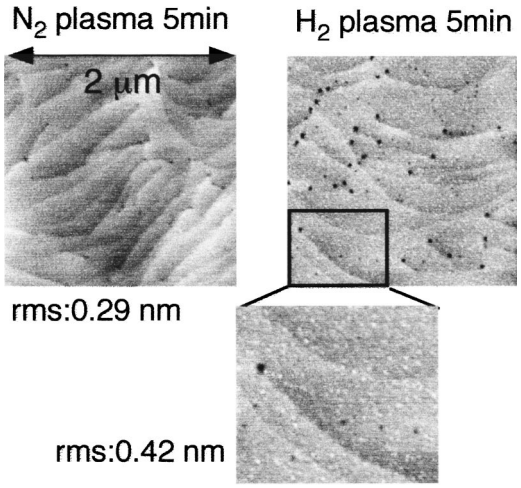

FIG. 4. AFM images of the ECR-plasma treated GaN surfaces.

correlated to the surface termination of the edge-screw mixed dislocations.[26] After the H_2-plasma treatment, however, the surface feature changed drastically. Large numbers of particles with diameters of about 20–30 nm were found on the treated GaN surface, as shown in the right-hand image in Fig. 4. From the XPS analysis, these particles were assigned to Ga droplets.

The surface state density (D_{SS}) distributions of the ECR-plasma treated GaN surfaces were compared in Fig. 5. The D_{SS} values were determined by the $C-V$ analysis (Terman method) using SiN_x-covered GaN samples. Except for the plasma treatments, the samples were processed under the same condition exactly. As clearly seen in Fig. 5, a localized surface level was found at approximately $E_c-0.5\,\mathrm{eV}$ for the H_2-plasma treated surfaces, while continuous D_{SS} distributions were observed in both the N_2-plasma treated surface and control sample without plasma treatment. Thus, the H_2-plasma treatment causes the formation of surface defects on the GaN surface.

In order to investigate the effects of plasma processing on the transport properties of 2DEG at GaN/AlGaN heterointerface, a gateless HFET structure shown in Fig. 6(a) was prepared.[27] The current–voltage ($I_{DS}-V_{DS}$) characteristics of the fabricated gateless HFET are shown in Fig. 6(b). We fabricated more than 100 devices on one chip of the GaN/AlGaN structure before plasma treatments. After measuring the initial $I-V$ characteristics of the devices, the chip was divided into two samples: one for the H_2-plasma treatment and the other for the N_2-plasma treatment. After the plasma treatments, we compared the $I-V$ characteristics for the certain devices that had the same initial $I-V$ characteristics. All the devices showed a steep linear increase of current followed by current saturation. After the H_2-plasma treatment for 1 min, a large current reduction was observed. On the other hand, N_2-plasma treatment slightly increased currents. The Hall measurement results showed that the change in currents after the plasma treatments was not due to change in mobility but due to the change in the 2DEG density. Additionally, the H_2-plasma-treated devices exhibited serious hysteresis in dc $I-V$ curves as well as transient behavior in pulse-responses of the drain currents.[27] These results indicate that the H_2-plasma treatment produced high-density surface defect states on the AlGaN surface, causing various kinds of instabilities in the 2DEG transport at GaN/AlGaN interface. No such effects were observed in the N_2-plasma treated devices.

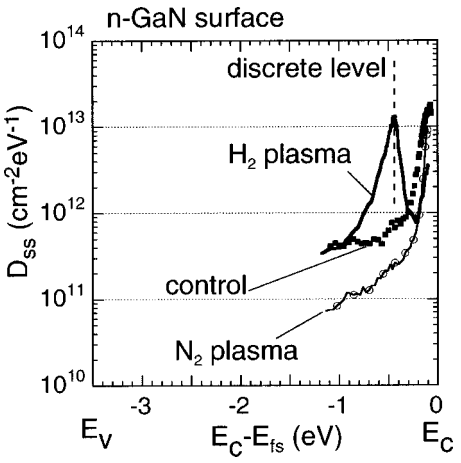

FIG. 5. Surface state density (D_{SS}) distributions of the ECR-plasma treated GaN surfaces.

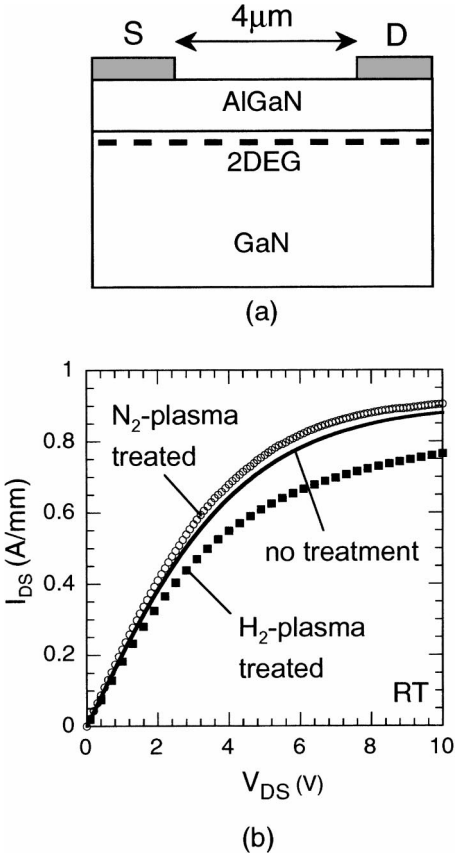

FIG. 6. (a) Gateless HFET structure and (b) current–voltage characteristics.

Figure 7 shows the XPS core-level spectra taken from the AlGaN surfaces after the treatments in H_2 plasma and N_2

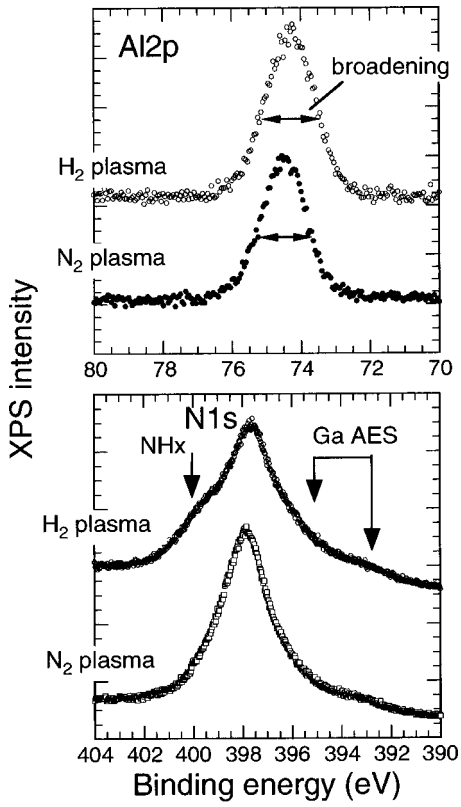

FIG. 7. XPS core-level spectra taken from the GaN/AlGaN surfaces after the treatments in ECR-excited H_2 plasma and N_2 plasma.

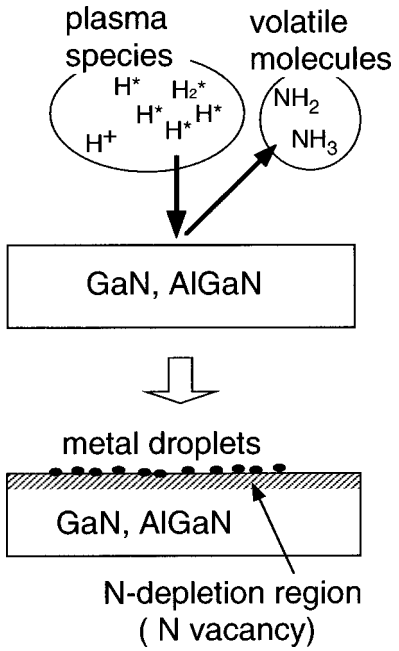

FIG. 8. Schematic illustration for a possible reaction process on GaN or AlGaN surfaces during the H_2-plasma treatment.

plasma for 1 min. We detected the photoemission from the AlGaN surfaces using an electron escape angle of 10°, implying that the obtained spectra reflected information from the topmost region (within 1.0–1.5 nm). In the N 1*s* core-level spectrum of the H_2-plasma treated sample, a clear shoulder peak appeared at around 399 eV, corresponding to the N–H_x bond.[28] In addition, the decrease in the peak intensity of the N 1*s* line was observed. The V/III ratio of the AlGaN surface after the H_2-plasma treatment was found to be far below unity (0.79), clearly indicating the depletion of N atoms at the surface. The broadening of spectrum was also observed in Al 2*p* core level. Thus, the H_2-plasma treatment for only 1 min produced disordered layer at the AlGaN surface with a highly nonstoichiometric chemical phase.

Figure 8 schematically shows a possible reaction process on GaN or AlGaN surfaces during the H_2-plasma treatment. It is expected that highly active hydrogen plasma species such as hydrogen radicals react with the surface to form volatile NH_x products, as manifested as a shoulder in the XPS N 1*s* spectrum (Fig. 7). This process led to the N depletion and left Ga and/or Al metallic clusters at the topmost GaN or AlGaN surfaces. Such a surface reaction process in H_2 plasma caused the formation of surface disordered layer and could introduce surface defect states including N–vacancy-related defects. Neugebauer and Van de Walle,[29] and Boguslawski *et al.*[30] have calculated energy levels of native point defects in GaN using the first-principle supercell method. They concluded that the simple N–vacancy creates resonant levels in the conduction band and contributes to the conduction band edge, supplying free electrons in GaN. On the other hand, recent results of calculation using the Green's function method by Yamaguchi and Junnarkar[31] predicted that the V_N defect can form an s-like discrete deep level within the gap. Thus, these suggest a possibility that N–vacancy-related clusters and/or defects may act as donor-type deep levels.

On the other hand, no such decrease of N atoms was observed after the N_2-plasma treatment, although it was also effective in removing oxides from the surface. As compared with the air-exposed AlGaN surface, the peak shift of 0.4–0.5 eV toward higher binding energies was observed in the Al 2*p* spectrum in the N_2-plasma treated AlGaN surface, as shown in Fig. 7. A similar peak shift was also observed in XPS core levels at the N_2-plasma treated GaN surface. These peak shifts indicate the reduction of the surface band bending.[9] Thus, the ECR-N_2 plasma treatment seems to partially recover or terminate surface defects, leading to the reduction of densities of surface states on GaN and AlGaN.

B. Surface passivation of GaN and GaN/AlGaN surfaces by SiO_2 and SiN_x

Electrical properties of the passivated GaN surfaces were investigated using MIS structures. Figure 9 shows typical $C-V$ curves obtained from the SiO_2/n-GaN and the SiN_x/n-GaN MIS structures where the dielectric films were deposited on the GaN surfaces after the ECR-N_2 plasma treatment. Also shown are the calculated curves based on the accumulation, depletion and inversion behavior for the MIS structure.[32] For calculation, an effective electron mass of

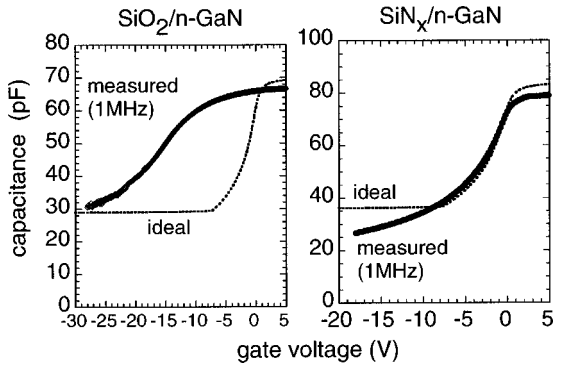

FIG. 9. Typical $C-V$ curves obtained from the SiO_2/n-GaN and SiN_x/n-GaN MIS structures prepared by ECR CVD. The GaN surfaces were treated in the N_2 plasma before the deposition of dielectric films.

$0.2\,m_0$, an effective hole mass of $0.8\,m_0$, a dielectric constant of 9.5 and an energy gap of 3.40 eV were used for GaN at room temperature.

Poor $C-V$ behavior was observed in the SiO_2-passivated sample, in spite of the fact that a natural oxide layer was almost removed from the GaN surfaces by the N_2-plasma treatment. A large discrepancy between the measured and calculated curves, including gradual slope in capacitance change from the accumulation region to the depletion region, indicates the existence of high-density interface states. In contrast, the SiN_x/GaN structure showed better $C-V$ characteristics. The measured $C-V$ curve was very close to the calculated one, and clear deep depletion behavior was observed even at room temperature. Similar deep depletion features with no inversion characteristics were reported in SiO_2/GaN (Ref. 22) and SiO_2/SiC systems,[33] because the generation rate of the minority carriers (holes in this case) is extremely low at room temperature in wide-gap semiconductor MIS systems. These results indicated that the SiN_x-gate control of surface potential was achieved over a remarkably wide within the bandgap of GaN.

Figure 10 shows distributions of interface state density (D_{it}) of the SiO_2/n-GaN and SiN_x/n-GaN structures, which

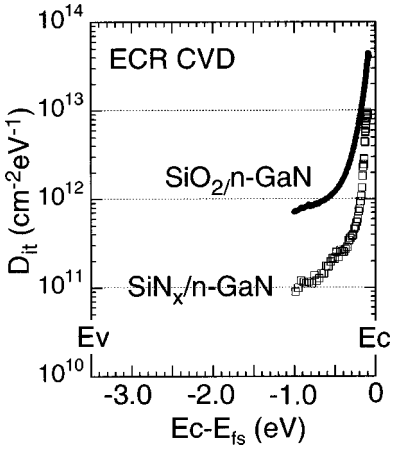

FIG. 10. Distributions of interface state density (D_{it}) of the SiO_2/n-GaN and SiN_x/n-GaN structures.

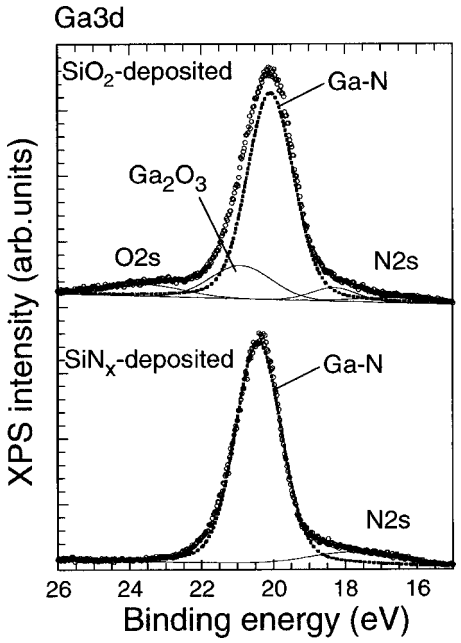

FIG. 11. *In situ* XPS Ga $3d$ spectra obtained from SiO_2- and SiN_x-deposited GaN surfaces. The thickness of insulating film is 2 nm.

were calculated by applying the Terman method to the measured $C-V$ curves at room temperature.[32] One of the essential conditions for the Terman method is that the change in interface charges corresponding to the state density can appear in the shift in the measured $C-V$ curve. For wide-gap semiconductors, however, there are some cases where this condition does not apply. It is expected, for example, that the states near midgap have large time constants for carrier emission. In this case, the charging state is remained almost unchanged during the gate voltage sweep even if the interface states have high densities. Thus, we estimated the limitation of applying the Terman method to calculation of interface state density in terms of the carrier emission time from the interface state at RT. The results showed that one cannot evaluate densities of interface states at the energies below E_C-1.0 eV from $C-V$ measurements at RT, due to the extremely long carrier emission times from the corresponding states.

As shown in Fig. 10, the presence of high-density interface states seriously disturb a smooth gate control of the surface potential for the SiO_2/n-GaN structure. We detected an interfacial Ga-oxide peak in XPS Ga $3d$ spectrum in the separate SiO_2/GaN sample having a very thin (2 nm) SiO_2 layer, as shown in Fig. 11(a). In the initial stage of the SiO_2 deposition, unexpected and uncontrollable oxidation reaction could take place at the GaN surface due to the supply of oxygen-related active ions and/or radicals. Formation of such an interfacial oxide is believed to be one of the reasons for the degradation of electrical properties of the SiO_2/GaN interface.

In comparison with the SiO_2/n-GaN interface, the SiN_x/GaN structures showed relatively low densities of interface states, as shown in Fig. 10. Since the control

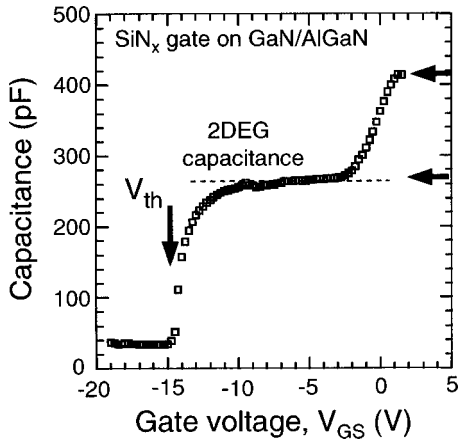

FIG. 12. $C-V$ characteristics of the SiN_x-gate structure formed on the GaN/AlGaN surface.

SiN_x/GaN sample without the N_2-plasma treatment showed higher D_{it} values ranging from 3×10^{11} to $5\times10^{11}\,cm^{-2}\,eV^{-1}$, the N_2-plasma treatment is effective in improving interface properties. No interfacial oxide was detected at the SiN_x/GaN interface, as shown in Fig. 11(b). Furthermore, the Raman spectra taken by the backscattering geometry at RT indicated no pronounced stress at the GaN surface covered with a SiN_x film.

The present SiN_x-based passivation was applied to the surface of GaN/AlGaN heterostructure. Figure 12 shows the $C-V$ characteristics of the SiN_x-gate structure formed on the GaN/AlGaN surface. The thickness of the SiN_x film is 41 nm and the electrode diameter is 600 μm. The measured $C-V$ curve clearly indicates a plateau region, reflecting the presence of 2DEG at the GaN/AlGaN interface. Thus, the capacitance value at the plateau region can easily be estimated from the total capacitance given by the AlGaN barrier capacitance and the SiN_x insulator capacitance. The estimated value was well in agreement with the experimental one. The maximum capacitance at round $V_{GS}=2$ V also corresponded to the SiN_x insulator capacitance. In addition, the experimental threshold voltage, V_{th}, is reasonably close to a simple estimation using $V_{th}=\Phi_B-qn_s/C_T$ (here, Φ_B is the potential barrier at the SiN_x surface, n_s is the 2DEG density and the C_T is the total capacitance in unit area). These results indicate that the SiN_x-insulated gate can control the potential in the AlGaN barrier layer, thereby leading to the expected modulation of the 2DEG density.

All these results indicated that the SiN_x-based passivation structure achieved good electronic properties of the GaN and AlGaN insulator–semiconductor interfaces. However, a negative issue appeared in the leakage characteristics. Figure 13(a) showed $I-V$ characteristics of the $Al/SiN_x/n\text{-}Al_{0.3}Ga_{0.7}N$ structure with the SiN_x thickness of 20 nm. For comparison, the $I-V$ curves of $Ni/n\text{-}Al_{0.3}Ga_{0.7}N$ and $Al/SiN_x/n\text{-}Si$ structures were plotted in Fig. 13(a). As expected, the SiN_x-insulated gate drastically reduced leakage currents in the reverse bias condition, as compared with the Schottky gate structure. For forward bias, however, a steep

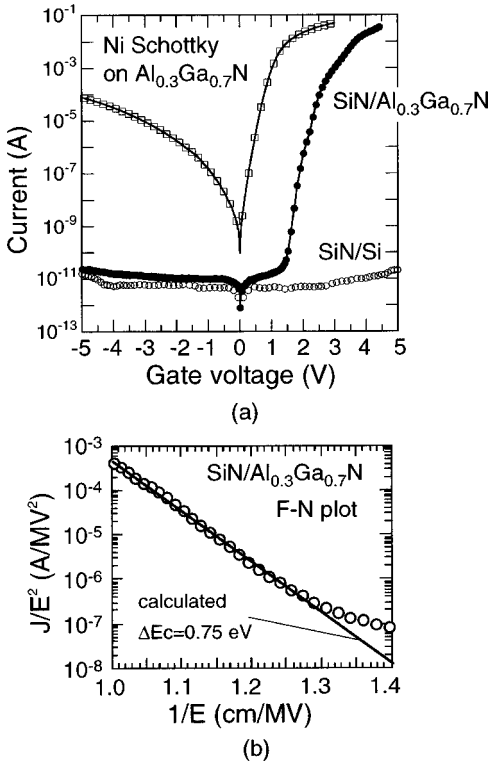

FIG. 13. (a) $I-V$ characteristics of the $Al/SiN_x/n\text{-}Al_{0.3}Ga_{0.7}N$ structure with the SiN_x thickness of 20 nm. For comparison, the $I-V$ curves of $Ni/n\text{-}Al_{0.3}Ga_{0.7}N$ and $Al/SiN_x/n\text{-}Si$ structures are plotted. (b) The plots of $\log(J/E^2)$ vs $1/E$ for the $SiN_x/n\text{-}Al_{0.3}Ga_{0.7}N$ structure.

increase of leakage current was observed at around $V_G=1.5$ V for the $SiN_x/n\text{-}Al_{0.3}Ga_{0.7}N$ system, while the $SiN_x/n\text{-}Si$ structure keeps the low level of leakage current. We have replotted the $I-V$ data at a large leakage region for the $Al/SiN_x/n\text{-}AlGaN$ structure in the form of $\log(J/E^2)$ vs $1/E$ (here, J is the current density and E is electric field). The result is shown in Fig. 13(b). The linear relation of $\log(J/E^2)$ vs $1/E$ indicates that the leakage is governed by the Fowler–Nordheim (FN) tunneling mechanism. From the fitting to this linear relation, we obtained the tunneling barrier height of 0.75 eV, corresponding to the conduction band offset, ΔE_C, between SiN_x and $Al_{0.3}Ga_{0.7}N$. In the fitting, we assumed the effective mass of electron in SiN_x to be $m_e^*=0.30\,m_0$ (m_0: electron rest mass), often used in the SiO_2/Si system.

In order to investigate a band alignment between SiN_x and $Al_{0.3}Ga_{0.7}N$, the XPS analysis was employed in the $SiN_x/Al_{0.3}Ga_{0.7}N$ structures. Figure 14(a) shows the N 1s spectrum obtained from a thick SiN_x film (20 nm) on $Al_{0.3}Ga_{0.7}N$. From the onset of the energy loss peak, we estimated the bandgap of SiN_x to be 4.9 eV. Miyazaki[34] reported the value of 4.75 eV for the SiN_x/Si structure. Then, we estimated the valence band offset, ΔE_V, between SiN_x and $Al_{0.3}Ga_{0.7}N$ also from the XPS analysis.[35,36] This was carried out by measuring the energy difference between the Si 2p and Al 2p core levels in the $SiN_x/Al_{0.3}Ga_{0.7}N$ structures having a thin SiN_x film (2 nm). The band alignment obtained is schematically shown in Fig. 14(b). A relatively small value of $\Delta E_C=0.7$ eV was obtained, and this is well in

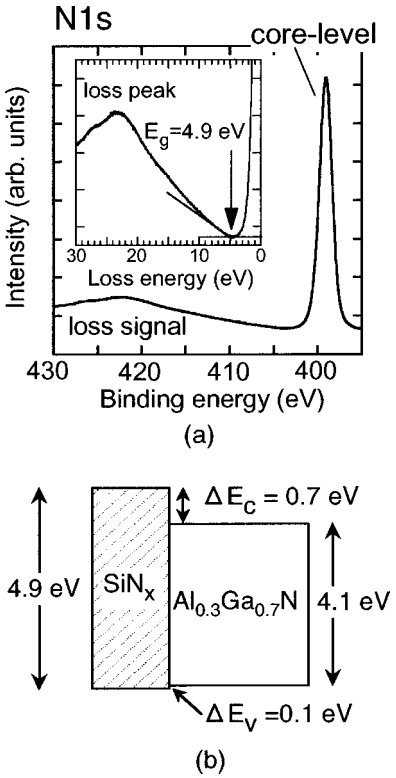

FIG. 14. (a) XPS N 1*s* spectrum obtained from a thick SiN_x film (20 nm) on $Al_{0.3}Ga_{0.7}N$ and (b) band alignment between SiN_x and $Al_{0.3}Ga_{0.7}N$.

agreement with that estimated by the F-N fitting method [Fig. 13(b)]. Thus, a serious leakage problem can arise from the band alignment at the $SiN_x/Al_{0.3}Ga_{0.7}N$ interface, thereby limiting the application of the SiN_x-based passivation structure to an insulated gate structure on GaN/AlGaN HFET system.

C. Novel Al_2O_3-based passivation structure

As described in the Introduction, an Al_2O_3 film has a large band gap, a large dielectric constant and a high breakdown field. This indicates an advantage of Al_2O_3 as an insulated gate for the GaN/AlGaN HFETs. In order to form a thin Al_2O_3 film on AlGaN and to control the Al_2O_3/AlGaN interface properties, we have employed the molecular beam deposition of Al and the subsequent ECR-O_2 plasma oxidation in *in situ* fashion.

The Al_2O_3 layer was fabricated through the following steps: The GaN/AlGaN surface was treated in NH_4OH solution at 50 °C for 10 min in air followed by the ECR-N_2 plasma treatment of the surface at 280 °C for 1 min. Then, an Al layer with a nominal thickness of 3 nm was deposited on the AlGaN surface at a deposition rate of 0.01 nm/s at RT in the MBE chamber (base pressure: 2×10^{-10} Torr). The top Al layer was then oxidized using ECR-excited O_2 plasma at RT for 5 min in the ECR CVD chamber. Finally, the sample was annealed at 700 °C for 10 min in the UHV annealing chamber. The AFM observation showed that the surface morphology maintained the smoothness with the characteristic feature dominated by monolayer steps, even after the passivation process. A comparable rms roughness value of 0.33 nm to the as-grown sample was obtained from the passivated AlGaN surface.

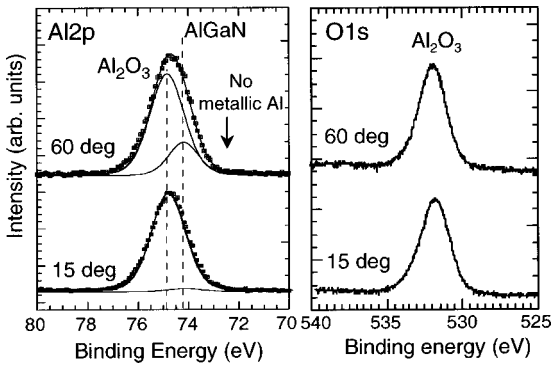

FIG. 15. XPS Al 2*p* and O 1*s* spectra obtained from the GaN/AlGaN surface after the formation of a thin Al_2O_3 film.

Figure 15 shows the XPS Al 2*p* and O 1*s* spectra obtained from the GaN/AlGaN surface after the formation of the thin Al oxide layer. In the Al 2*p* spectra, no metallic Al peak was detected. The peak could be deconvoluted into two components corresponding to the Al–O bond and the Al–N bond. The Al–N peak intensity increased with an escape angle of photoelectrons. On the other hand, the Al–O peak intensity almost remained unchanged, similar to the behavior of the O 1*s* peak. Furthermore, we confirmed no change in the spectra of Ga- and N-core levels before and after the formation process. These results indicated that a thin Al oxide layer was successfully formed on the top of GaN/AlGaN surface without disordering the chemical properties of the underneath AlGaN surface. From the comparison of integrated intensity ratios of O 1*s* to Al 2*p* between the formed Al oxide and a crystalline sapphire substrate as a standard, the composition of the present Al oxide was found to be Al_2O_3. The thickness of the Al_2O_3 layer was estimated to be 3.5 nm from the angle-resolved analysis of the Al 2*p* core-level intensities.

Figures 16(a) and 16(b) show the XPS O 1*s* spectrum of the Al_2O_3-passivated GaN/$Al_{0.3}Ga_{0.7}N$ surface and the valence-band spectra of the surface before and after the passivation. The band gap, E_G, of the thin Al_2O_3 layer can be determined from the onset position of the energy loss peak in the O 1*s* spectrum. As shown in Fig. 16(a), this analysis gave $E_G=7.0$ eV. The valence band spectrum before the passivation showed a characteristic feature of ''free'' AlGaN surface consisting of Ga 4*s*, Al 3*p*, and N 2*p* orbits.[35] After the surface passivation, a drastic change in the spectrum appeared, reflecting the formation of the Al_2O_3 layer. The valence band offset, ΔE_V, was estimated to be 0.8 eV from the energy difference between the leading edges of the valence-band spectra before and after the passivation, as shown in Fig. 16(b). From the values $E_G=4.1$ eV for $Al_{0.3}Ga_{0.7}N$, $E_G=7.0$ eV for Al_2O_3, and $\Delta E_V=0.8$ eV, the conduction band offset, ΔE_C, was estimated to be 2.1 eV. The obtained band alignment between Al_2O_3 and $Al_{0.3}Ga_{0.7}N$ is shown in Fig. 16(c).

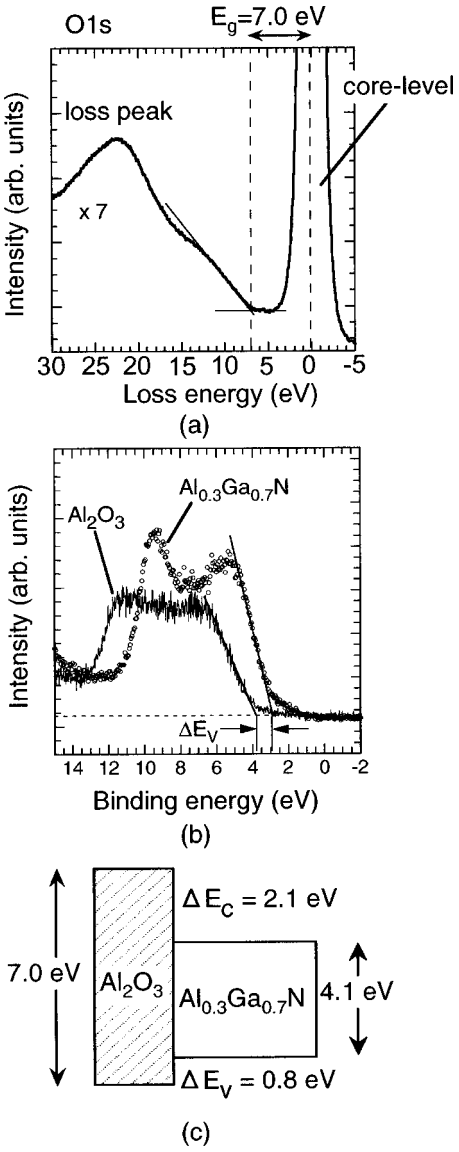

FIG. 16. (a) XPS O 1*s* spectrum of the Al_2O_3-passivated $Al_{0.3}Ga_{0.7}N$ surface, (b) the valence-band spectra of the $Al_{0.3}Ga_{0.7}N$ surface before and after the passivation, and (c) band alignment between Al_2O_3 and $Al_{0.3}Ga_{0.7}N$.

This band structure led to the reduction of leakage currents at forward bias as compared with the Ni-Schottky gate and the SiN_x-insulated gate structures, as shown in Fig. 17, in spite of a very small thickness of the Al_2O_3 layer of 3.5 nm. A slope of gradual increase in leakage current for the Al_2O_3-insulated gate at forward bias is less than that of the SiN_x-insulated gate, indicating a direct tunneling mechanism in leakage through the Al_2O_3 layer rather than the FN tunneling.

D. Application of the Al_2O_3-based passivation structure to insulated-gate GaN/AlGaN HFET

The present Al_2O_3-based passivation structure was applied to the fabrication of an insulated-gate type GaN/AlGaN HFET. The device structure is schematically shown in Fig. 18. After the device isolation and Ohmic electrode metallization, the surface of GaN/AlGaN HFET structure was passivated by the thin Al_2O_3 layer through a process described in the previous section. Subsequently, the submicron metal-gate patterns were defined and fabricated by a combination of electron-beam lithography and lift-off techniques.

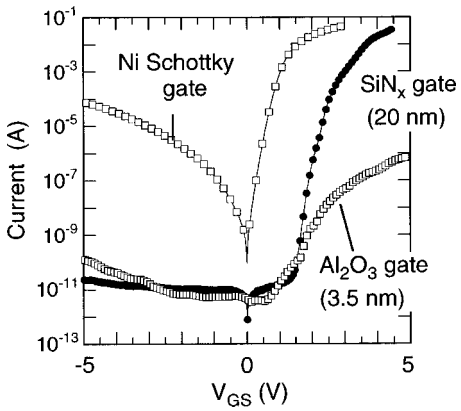

FIG. 17. $I-V$ characteristics of the Ni-Schottky gate, SiN_x-insulated gate and Al_2O_3-insulated gate structures.

Figure 19 shows typical drain $I-V$ characteristics of the fabricated Al_2O_3 insulated-gate (IG) HFET and Schottky-gate (SG) HFET with a gate length of 0.4 μm. The Al_2O_3 IG HFET showed a good gate controllability up to $V_{GS}=+3$ V and achieved high drain saturation current of about 0.8 A/mm, as shown in Fig. 19(a). These characteristics are better than SG HFET. The observed maximum g_m value is 120 mS/mm.

We investigated current collapse characteristics under a quiescent gate voltage stress.[19] The result is shown in Fig. 20. During the measurement, the drain voltage, V_{DS}, was kept at 15 V. First, we set the initial gate voltage as $V_{GS0}=0$ V for 10 s. After that, V_{GS} was switched to $+1$ V instantaneously and then decreased to -8 V with a sweeping rate of 0.2 V/s. This measurement mode is indicated by "normal mode" in Fig. 20. In the "stress mode," on the other hand, we applied $V_{GS}=-8$ V (far below the threshold voltage) for 10 s as the initial stress of the gate voltage. Then, the V_{GS} sweeping was carried out from $+1$ V to -8 V. As shown in Fig. 20(a), a significant collapse was observed more than 10% in the drain currents for the SG HFET. On the other

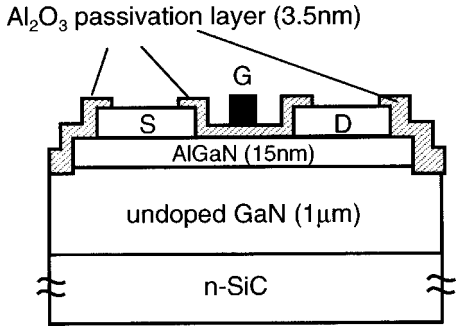

FIG. 18. Schematic illustration of insulated-gate type GaN/AlGaN HFETs with the Al_2O_3-based surface passivation structure.

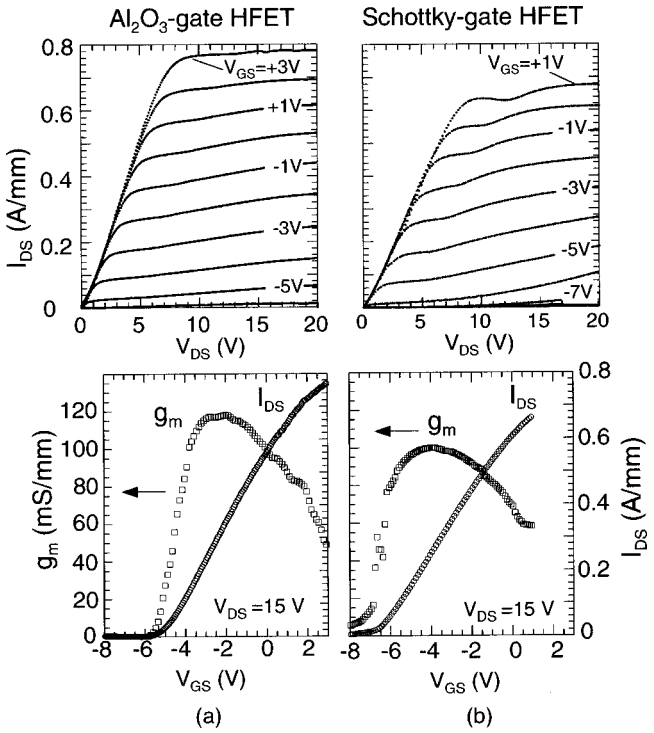

FIG. 19. $I-V$ characteristics of the fabricated (a) Al_2O_3 insulated-gate (IG) HFET and (b) Schottky-gate (SG) HFET with a gate length of 0.4 μm.

hand, no current collapse was observed for the IG HFET. This indicates a remarkable advantage of the present Al_2O_3-based passivation structure.

The current collapse effects have often been observed GaN/AlGaN SG HFETs under quiescent gate stress[19] or pulse-mode gate stress.[17,18,24,37] The collapse is also induced by drain stress.[1,18,37] The mechanism for the current collapse is not clarified yet. Since a SiN_x-based surface passivation dramatically reduces the current collapse,[1,17–19] some models based on the electron trapping by surface states have been proposed.[1,19] As described in the Sec. III A, the H_2-plasma treatment produces N–vacancy related defects on GaN and AlGaN surfaces. We have also found that the ECR-N_2 plasma treatment is very effective in suppressing the formation of such N–vacancy-related surface defects.[9,27] Based on these findings, Hasegawa and co-workers[27,38,39] have recently proposed a unified surface model that the electronic states consisting of N–vacancy related surface levels and U-shaped surface state continuum are responsible for the electron trapping on GaN/AlGaN heterostructure surfaces. In case of SG HFETs, electrons can be injected into the surface states assisted by large leakage currents under the deep gate stress. The present Al_2O_3-based passivation process including ECR-N_2 plasma treatment can suppress the formation of N–vacancy related near-surface levels as well as surface states. In addition, the Al_2O_3 IG structure remarkably reduces the gate leakage currents. Thus, our Al_2O_3-based insulated gate and surface passivation structure is very effective in suppressing the current collapse effects, thereby leading to the reliability improvement of AlGaN/GaN HFETs.

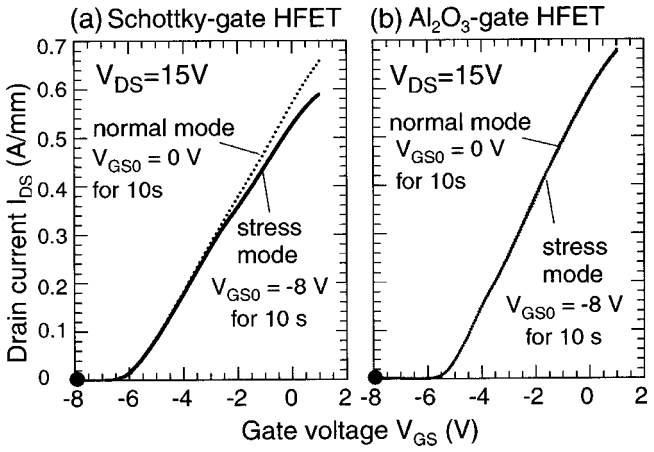

FIG. 20. $I_{DS}-V_{GS}$ characteristics of (a) the Schottky-gate HFET and (b) the Al_2O_3 insulated-gate HFET before and after the gate stress. V_{GS0} indicates the initial gate voltage stress.

IV. CONCLUSION

We have investigated the effects of plasma processing, formation of Si-based dielectrics and formation of a thin Al_2O_3 film on the chemical and electronic properties of GaN and AlGaN surfaces. The ECR-H_2-plasma treatment was found to produce nitrogen–vacancy-related defect levels at GaN and AlGaN surfaces, while the treatment in ECR-N_2 plasma improved the electronic properties of surfaces. The deposition of SiO_2 film on GaN and AlGaN surfaces induced high-density interface states, due to unexpected and uncontrollable oxidation reactions on the surfaces during the deposition process. In comparison, the SiN_x/GaN passivation structure prepared by ECR CVD with the N_2-plasma pretreatment showed good interface properties with the minimum D_{it} value of $1\times10^{11}\,cm^{-2}\,eV^{-1}$. No pronounced stress remained at the SiN_x/GaN interface. Excess leakage currents based on the Fowler–Nordheim tunneling were observed in the $SiN_x/Al_{0.3}Ga_{0.7}N$ structure, due to a relatively small conduction band offset, ΔE_C, of 0.7 eV between SiN_x and $Al_{0.3}Ga_{0.7}N$. A novel Al_2O_3-based passivation structure was successfully formed on the AlGaN surface by molecular beam deposition of Al and the subsequent ECR-O_2-plasma oxidation. *In situ* XPS analysis showed a band gap of 7.0 eV for the formed Al_2O_3 layer with a thickness of 3.5 nm and a sufficiently large ΔE_C of 2.1 eV between Al_2O_3 and $Al_{0.3}Ga_{0.7}N$. The GaN/AlGaN insulated-gate HFETs having the Al_2O_3-based passivation structure showed a good gate control of drain currents up to $V_{GS}=+3$ V and achieved drain saturation current of 0.8 A/mm. The observed maximum g_m value is 120 mS/mm. No current collapse was observed in the Al_2O_3 IG HFETs. These results indicate a remarkable advantage of the present Al_2O_3-based passivation structure for GaN/AlGaN HFETs, leading to the reliability improvement of AlGaN/GaN HFETs.

ACKNOWLEDGMENTS

This work was partly supported by the 21C COE Project on ''Meme-Media Based Next Generation ITs'' and grant-in-aid for Scientific Research (B) (No. 14350155) from the Ministry of Science, Education, Sports, and Culture, Japan.

[1]R. Vetury, N. Q. Zhang, S. Keller, and U. K. Mishra, IEEE Trans. Electron Devices **48**, 560 (2001).
[2]M. A. Kahn, X. Hu, A. Tarakji, G. Simin, J. Yang, R. Gaska, and M. S. Shur, Appl. Phys. Lett. **77**, 1339 (2000).
[3]E. J. Miller, X. Z. Dang, and E. T. Yu, J. Appl. Phys. **88**, 5951 (2000).
[4]E. D. Readinger, B. P. Luther, S. E. Mohney, and E. L. Piner, J. Appl. Phys. **89**, 7983 (2001).
[5]S. W. King, J. P. Bamak, M. D. Bremser, K. M. Tracy, C. Ronning, and R. F. Davis, J. Appl. Phys. **84**, 5248 (1998).
[6]P. J. Hartlieb, A. Roskowski, R. F. Davis, A. Platow, and R. J. Nemanich, J. Appl. Phys. **91**, 732 (2002).
[7]T. Hashizume, S. Ootomo, R. Nakasaki, S. Oyama, and M. Kihara, Appl. Phys. Lett. **76**, 2880 (2000).
[8]T. Hashizume, R. Nakasaki, S. Ootomo, S. Oyama, and H. Hasegawa, Mater. Sci. Eng., B **80**, 309 (2001).
[9]T. Hashizume, S. Ootomo, S. Oyama, M. Konishi, and H. Hasegawa, J. Vac. Sci. Technol. B **19**, 1675 (2001).
[10]S. C. Binari, L. B. Rowland, G. Kelner, W. Kruppa, H. B. Dietrich, K. Doverspike, and D. K. Gaskill, Proceedings of the 21st International Symposium on Compound Semiconductors, San Diego (1994).
[11]H. Kawai, M. Hara, F. Nakamura, and S. Imanaga, Electron. Lett. **34**, 592 (1998).
[12]S. Imanaga, F. Nakamura, and H. Kawai, Jpn. J. Appl. Phys., Part 1 **40**, 1194 (2001).
[13]T. Hashizume, R. Nakasaki, and H. Hasegawa, Abstracts of 41st Electronic Materials Conference (1999), p. 29.
[14]R. Nakasaki, T. Hashizume, and H. Hasegawa, Physica E (Amsterdam) **7**, 953 (2000).
[15]B. M. Green, K. K. Chu, E. M. Chumbes, J. A. Smart, J. M. Shealy, and L. F. Eastman, IEEE Electron Device Lett. **21**, 268 (2000).
[16]J.-S. Lee, A. Vescan, A. Wieszt, R. Dietrich, H. Leier, and Y.-S. Kwon, Tech. Dig. - Int. Electron Devices Meet. 381 (2000).
[17]X. Hu, A. Koudymov, G. Simin, J. Yang, M. A. Khan, A. Tarakji, M. S. Shur, and R. Gaska, Appl. Phys. Lett. **79**, 2832 (2001).
[18]T. Kikkawa, M. Nagahara, N. Okamoto, Y. Tateno, Y. Yamaguchi, N. Hara, K. Joshin, and P. M. Asbeck, Tech. Dig. - Int. Electron Devices Meet. 585 (2001).
[19]T. Mizutani, Y. Ohno, M. Akita, S. Kishimoto, and K. Maezawa, Phys. Status Solidi A **194**, 447 (2002).
[20]R. Therrien, G. Lucovsky, and R. Davis, Appl. Surf. Sci. **166**, 513 (2000).
[21]M. Hong, K. A. Anselm, J. Kwo, H. M. Ng, J. N. Baillargeon, A. R. Kortan, C. M. Lee, J. I. Chyi, and T. S. Lay, J. Vac. Sci. Technol. B **18**, 1453 (2000).
[22]B. Gaffey, L. J. Guido, X. W. Wang, and T. P. Ma, IEEE Trans. Electron Devices **48**, 458 (2001).
[23]K. Inoue, Y. Ikeda, H. Masato, T. Matsuno, and K. Nishi, Tech. Dig. - Int. Electron Devices Meet. 577 (2001).
[24]B. Luo, J. W. Johnson, J. Kim, R. M. Mahandru, F. Ren, B. P. Gila, A. H. Onstine, C. R. Abernathy, S. J. Pearton, A. G. Baca, R. D. Briggs, R. J. Shul, C. Monier, and J. Han, Appl. Phys. Lett. **80**, 1661 (2002).
[25]Z. Jin, T. Hashizume, and H. Hasegawa, Appl. Surf. Sci. **190**, 361 (2002).
[26]B. Heying, E. J. Tersa, C. R. Elsas, P. Fini, S. P. DenBaars, and J. S. Speck, J. Appl. Phys. **85**, 6470 (1999).
[27]T. Inagaki, T. Hashizume, and H. Hasegawa, Appl. Surf. Sci. (in press).
[28]X. Y. Zhu, M. Wolf, and J. M. White, J. Vac. Sci. Technol. A **11**, 838 (1993).
[29]J. Neugebauer and C. G. Van de Walle, Phys. Rev. B **50**, 8067 (1994).
[30]P. Boguslawski, E. L. Briggs, and J. Bernholc, Phys. Rev. B **51**, 17255 (1995).
[31]E. Yamaguchi and M. R. Junnarkar, J. Cryst. Growth **189/190**, 570 (1998).
[32]E. H. Nicollian and J. R. Brews, *MOS Physics and Technology* (Wiley, New York, 1982), Chap. 8.
[33]A. Link, K. Bitzer, W. Limmer, R. Sauer, C. Kirchner, V. Schwegler, M. Kamp, D. G. Ebling, and K. W. Benz, J. Appl. Phys. **86**, 6256 (1999).
[34]S. Miyazaki, J. Vac. Sci. Technol. B **19**, 2212 (2001).
[35]J. R. Waldrop and R. W. Grant, Appl. Phys. Lett. **68**, 2879 (1996).
[36]S. W. King, C. Ronning, R. F. Davis, M. C. Benjamin, and R. J. Nemanich, J. Appl. Phys. **84**, 2086 (1998).
[37]K. Kunihiro, K. Kasahara, Y. Takahashi, and Y. Ohno, Jpn. J. Appl. Phys., Part 1 **39**, 2431 (2000).
[38]H. Hasegawa and S. Oyama, J. Vac. Sci. Technol. B **20**, 1647 (2002).
[39]H. Hasegawa, S. Ootomo, T. Inagaki, and T. Hashizume, J. Vac. Sci. Technol. B, these proceedings.